Temperature sensor based on selective liquid-filled twin-core photonic crystal fiber

Chenlu Wang [a,b,c,] Perry Ping Shum [a, b*], Dora Juan Juan Hu[c*] Zhilin Xud, Shuhui Liu[e], Yongwei Zhu[c] Yu Zheng [a, b], Baocheng Li [a, b], Chen Yang [f,g], Weijun Tong[f,g], Yue Meng[f,g], Georges Humbert[h]

[a] CINTRA CNRS/NTU/THALES, UMI 3288, 639798, Singapore; [b] School of Electrical and Electronic Engineering, Nanyang Technological University, 639798, Singapore; [c] Institute for Infocomm Research, A*STAR, Singapore; [d] MOE Key Laboratory of Fundamental Physical Quantities Measurement & Hubei Key Laboratory of Gravitation and Quantum Physics, PGMF and School of Physics, Huazhong University of Science and Technology, Wuhan 430074, P. R. China; [e] Hubei Key Laboratory of Optical information and Pattern Recognition, Wuhan Institute of Technology, Wuhan 430205, China ; [f] Yangtze Optical Fibre and Cable Joint Stock Limited Company; [g] The State Key Laboratory of Optical Fibre and Cable Manufacture Technology (SKLOFCMT); [h] XLIM Research institute, UMR CNRS / University of Limoges, 123 av. A. Thomas, 87060, Limoges, France.

ABSTRACT

We experimentally demonstrated a temperature sensor by selectively infiltrating refractive index oil (RIMO) in the central airhole of a twin-core photonic crystal fiber (TCPCF). The light incident in the central liquid core effectively enhanced the power coupling between two solid cores under phase-matching condition over a short coupling length. A large spectrum envelop was extracted by a low pass filter from the transmission spectrum. By tracing the wavelength shifts of the large envelop, the largest sensitivity is 34.561 nm/℃ within the temperature range from 54 ℃ to 55 ℃. This ultrahigh temperature sensitivity benefited from the interference between fundamental hybrid supermodes of the RIMO infiltrated structure. While the refractive index (RI) of the central liquid core was decreasing with the increasing temperature, the coupling among two solid cores and the central liquid core can still be observed but with a lower power coupling efficiency, whereas the temperature sensitivity became 19.413 nm/℃ from 55 ℃ to 58.2 ℃.

Keywords: Fiber sensor, selective liquid infiltration, optofluidic, temperature sensor, Twin-core Photonic crystal fiber, supermodes interference, three parallel waveguide structure.

1. INTRODUCTION

Recent development on optofluidic, as a combination of fluidics and photonics, has been paid a lot of attention nowadays. Its irreplaceable advantages, such as fast responsibility, good adaptability, and easy accessibility, lead to many attractive optofluidic applications based on the integration with optical fibers [1-2]. After the Photonic Crystal Fibers (PCFs) were first reported in 1995, they were explored and developed as an attractive platform in sensing applications compared with conventional fiber due to their unique features [3]. One of the most important characteristics of PCF is the high flexibility of the geometrical fiber design. The holey structure of the PCF cladding provides a natural platform for their

infiltration with various sorts of liquids, such as RIMO [4-7], liquid crystal [9-10], and magnetic fluid [11-12] which can significantly enhance the tunability and sensitivities of optical devices.

Sensitivity is the most important parameter to evaluate sensor performance. One of the methods to enhance the sensitivity of a fiber-based sensing device is to introduce a two-core structure in the PCF as an in-fiber coupler to generate sharp resonances [1]. In previous studies, a series of investigations focused on post-processing of TCPCF as a Mach–Zehnder interferometer (MZI) structure for sensing applications. By selectively filling part of the TCPCF, a temperature sensor with temperature sensitivity up to 5.43 nm/°C was achieved by Hou, M., et al [13]. Besides, a hybrid TCPCF temperature sensor was reported by Zhilin Xu, et al., with the first ring of airholes surrounding one of the silica cores of the TCPCF filled with liquid crystal, temperature sensitivity can be reached to 4.91 nm /°C and −3.68 nm/°C for nematic phase, and isotropic phase of proposed liquid crystal, respectively [10].

With optimized liquid infiltration design by using liquid with a high thermo-optic coefficient, as well as a data post-processing method, ultrahigh temperature sensitivity can be achieved based on optofluidic TCPCF. In this letter, we proposed an ultra-sensitive temperature sensor based on RIMO infiltration into the central airhole of the TCPCF. The central liquid-filled waveguide acted as a bridge, leading to enhanced power transfer between two solid cores over a wide temperature detectable range. A multi-component interference pattern was observed with a large envelop spectrum and fine fringe interference. Numerical simulation revealed the large envelop pattern resulted from the coupling between hybrid supermodes of the three parallel waveguides structure. By tracing the wavelength shift of the large envelop spectrum with the variation of temperature, the largest sensitivity calculated to be 34.561 nm/℃ with the temperature range from 54 ℃ to 55 ℃, and the temperature sensitivity is up to 19.413 nm/℃ from 55 ℃ to 58.2 ℃.

2. SENSOR FABRICATION AND OPERATION PRINCIPLE

2.1 Selective infiltration of TCPCF

A commercially available TCPCF was used in the experiment. The cross-sectional view of the TCPCF is shown in Fig.1 with airhole diameter is 2.3 μm and hole to hole spacing is 4 μm.

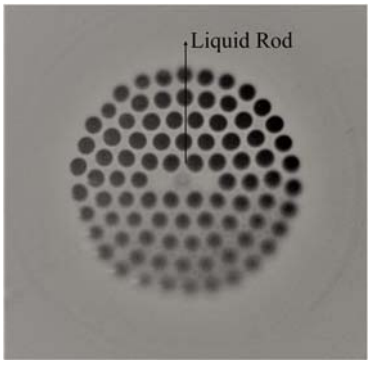

Figure 1.Selectively liquid infiltrated in the central airhole of twin-core photonic crystal fiber

The central liquid core was selectively infiltrated by RIMO with 1.46-RI at room temperature (Cargille Labs), and temperature-RI coefficient of -0.000398 RIU/ ℃. The selective infiltration method in the experiment directly blocked the airholes by UV glue and left only the central airhole open for RIMO infiltration as the following steps. Firstly, the TCPCF was fixed under a microscope. A tapered single

mode fiber (SMF) was then fixed by a 3D stage, to cover all the cladding airholes by UV glue through the SMF tip, except the central airhole. The final step achieved selective liquid infiltration by putting the UV glue to cover TCPCF end in the RIMO after the UV glue was solidified by UV light. The TCPCF with only central airhole filled with RIMO realizes by capillary effect with the cross-section view as shown in Fig.1.

2.2 Numerical supermode investigation and working principle

Due to the large thermo-optic coefficient of the proposed RIMO, the RI of the liquid decreased dramatically with the increase of temperature. When the temperature reached to around 54 ℃, the RI of the RIMO matched with the value of silica and formed a three-parallel-waveguide structure. Besides, the introduction of the central liquid core allowed a large overlap of the mode field and generated a series of supermodes [14-16]. The first three supermode field distribution were as shown in Fig.2 (a)-(c) in a sequence of symmetric mode, decoupling mode and anti-symmetric mode. For simplification, only x polarization was plotted, and the white arrow lines presented the direction of the electric field. The RI of silica was calculated by the Sellmeier equation with the consideration of both temperature and material dispersion [17]. The unavoidable airhole collapse at the surface of SMF and liquid filled TCPCF induced by splicing, enabled the recombination of different supermodes at the splicing point, resulting in an interference pattern in the transmission spectrum [18].

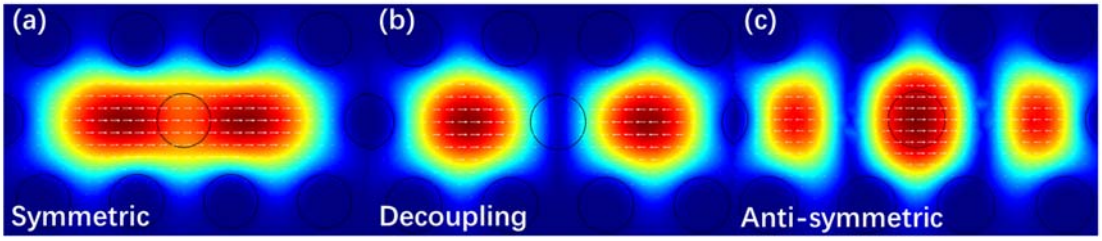

Figure 2. The first three fundamental hybrid supermodes field distribution of the three-waveguide structure: (a) symmetric mode; (b) decoupling mode; (c) antisymmetric mode, only x polarization has been plotted, the white dash lines indicate electrical field distribution.

To have a better understanding of the hybrid supermodes in the liquid filled TCPCF structure, the dispersion curve of the three-fundamental hybrid supermodes were plotted under 54 ℃ with the help of COMSOL as shown in Fig.3(a). The numerical wavelength range setting from 1250 nm to 1650 nm according to the experimental condition.

In the experiment, we ignored the thermal expansion influences, which had a limited impact on temperature sensitivity compared with the thermo optic effect [19]. Therefore, the temperature sensitivity of the proposed structure was expressed as Eq.1, with the assumption that L(T) remained constant [20].

$$\frac{\partial \lambda_{dip}}{\partial T} = -\frac{\lambda_0}{n_1(T) - n_2(T)}\left(\frac{\partial n_1(T)}{\partial T} - \frac{\partial n_2(T)}{\partial T}\right) \qquad (1)$$

Where ∂n1 (T)/∂T and ∂n2 (T)/∂T are the thermo optic coefficients of the two hybrid supermodes, respectively. Eq.1 indicated the temperature sensitivity depended on not only the index contrast of different supermodes, but the RI variation with temperature change. Therefore, we numerically simulated the RI variation of these three fundamental supermodes at 1440 nm with temperature range from 54 ℃ to 55 ℃ as shown in Fig.3(b)

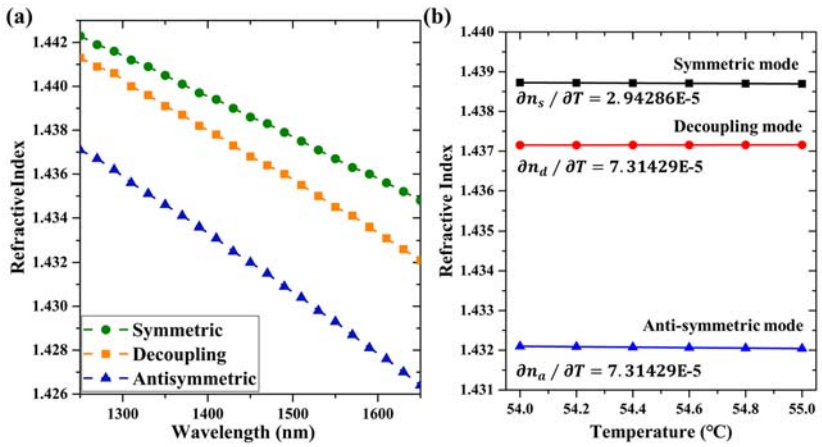

Figure 3. (a) Dispersion curve of the first three supermodes under 54 ℃; (b) Refractive index variation of three fundamental supermodes at wavelength equals to 1440 nm.

These three fundamental supermodes can be treated as the mode field superposition of fundamental core mode of TCPCF and LP01 mode of the central liquid rod, according to the coupled mode theory [15]. The power intensity of these three fundamental supermodes were expressed as the equations below:

$$\overrightarrow{A_s} = \frac{A_0}{\sqrt{2}} \cdot \frac{e^{i\sqrt{\kappa_1^2+\kappa_2^2}z}}{\sqrt{\kappa_1^2+\kappa_2^2}} \begin{pmatrix} \kappa_1 \\ \sqrt{\kappa_1^2+\kappa_2^2} \\ \kappa_2 \end{pmatrix} \tag{3}$$

$$\overrightarrow{A_d} = \frac{A_0}{\sqrt{\kappa_1^2+\kappa_2^2}} \begin{pmatrix} \kappa_1 \\ 0 \\ \kappa_2 \end{pmatrix} \tag{4}$$

$$\overrightarrow{A_a} = \frac{A_0}{\sqrt{2}} \cdot \frac{e^{-i\sqrt{\kappa_1^2+\kappa_2^2}z}}{\sqrt{\kappa_1^2+\kappa_2^2}} \begin{pmatrix} \kappa_1 \\ -\sqrt{\kappa_1^2+\kappa_2^2} \\ \kappa_2 \end{pmatrix} \tag{5}$$

Where, $\overrightarrow{A_s}$, $\overrightarrow{A_d}$, and $\overrightarrow{A_a}$ were eigenmodes, labeled as symmetric mode, decoupling mode and anti-symmetric mode [16]. With the total initial power $P_0 = |A_0|^2$ launched into the central liquid core, κ_1, $\kappa_2$is the coupling coefficient between the solid core and the central liquid core, ignored the slight difference might be induced by experimental operationa such as cleave angle, we assumed the $\kappa_1$is equal to $\kappa_2$in our experiment.

In particular, the power amplitude of the decoupling mode kept constant along with the propagation according to the Eq.2, which indicated the light energy was confined in the two solid cores without energy transfer through liquid-core. While the amplitudes of power in symmetric mode and antisymmetric mode were highly influenced by the central liquid core. Since the refractive index of the central liquid core was highly temperature-dependent due to the large thermo-optic coefficient of RIMO [21]. Therefore, the index contrast between different supermodes varied with the change of temperature, leading to a wavelength shift of the interference pattern. Therefore, the temperature sensitivity can be measured by tracking the wavelength shift of the interference feature point with the variation of temperature.

3. Experiment setup and conclusion

3.1 Experiment setup

The small separation between the liquid rod and two solid cores, leading to a large mode field overlap. Therefore, the interference between different hybrid supermodes was significantly enhanced, which resulted in a multipeak resonant pattern with narrow free space range (FSR). In an interference pattern, the relationship between FSR and the RI of supermodes involved in the interference as shown in Eq.6

$$FSR = \frac{\lambda^2}{|n_1 - n_2|L} \tag{6}$$

Where, n_1 and n_2 represented the effective RI of the two supermodes that involved in the interference, and L here represented the length of liquid filled TCPCF [22]. In order to achieve a large FSR as well as ensure the compactness of the device, the liquid filled TCPCF, was well cleaved to 1.8 cm with RIMO fully filled inside of the central airhole.

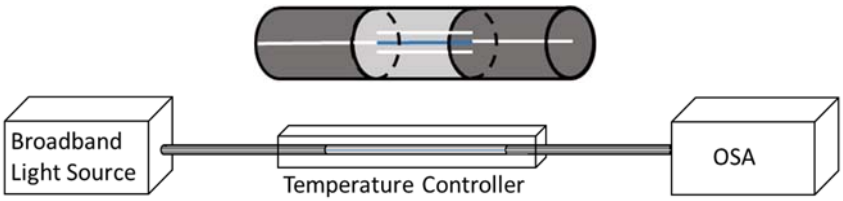

Figure 4. The schematic experiment setup

The experiment setup is shown as Fig. 5, by splicing the liquid filled TCPCF with two pieces of SMF at both fiber-ends with an optimized splicing setting. The liquid filled TCPCF was then fixed inside of a temperature controllable oven. The incident light from a broadband light source, and the transmission spectrum was collected by an optical spectrum analyzer (OSA) when the sample was heated. In our experiment, the temperature characteristic of the proposed temperature sensor was heated from 54 ℃ to 58.2 ℃ with a step of 0.2 ℃, by placing the liquid filled TCPCF in a temperature-controlled container [23].

3.2 Experiment results and conclusion

A multi-component transmission spectrum contained two sets of interference fringe pattern has been recorded. Fig.5(a). shows the transmission spectrum at 54 ℃ and 54.4 ℃, respectively. The interference fringe pattern of the proposed liquid filled TCPCF as shown in the solid line, caused by complicated interference between a series of modes. Instead of directly monitoring the wavelength shift of the featured points, a large envelop over broad wavelength range has been extracted by a low pass filter [24-25]. Shown as the brown dashed line and the purple dashed line at 54 ℃ and 54.4℃, respectively. As the temperature increase, dip A, shown as the triangle shape at the dip of large envelop spectrum experienced a dramatic wavelength shift from 54 ℃ to 54.4 ℃.

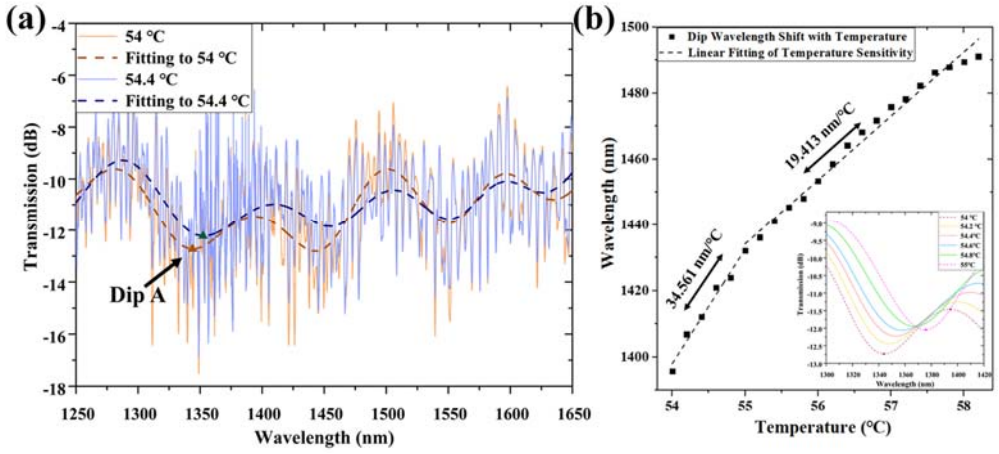

Figure 5. (a) Transmission spectra of the proposed multi-components interference sensor at 54°C and 54.4°C, with liquid filled TCPCF length of 1.8 cm; (b) Temperature sensitivity over the temperature range from 54 °C to 58.2 °C. The insert figure shows dip wavelength shifts as a function of temperature from 54 °C to 55 °C.

The temperature sensitivity was measured by tracing the wavelength shift of the large spectrum envelop with temperature variation. The temperature sensitivity of the proposed structure was recorded and plotted as Fig.5(b) from 54 °C to 58.2 °C, the insert figure represented the dip wavelength shifts as a function of temperature from 54 °C to 55 °C. As shown in Fig.5(b) that the temperature sensitivity was up to 34.561 nm/°C within a temperature range from 54 °C to 55 °C, and then the sensitivity was19.413 nm/°C from 55°C to 58.2 °C.

Based on Eq.1 and Eq.6, the supermodes that involved in the interference within different temperature ranges can be decided by the experimental results of FSR. With temperature ranges from 54 °C to 55 °C, the refractive index difference $\Delta n = 0.0013794$, calculated from FSR equaled 81.857 nm. According to the previous numerical investigation on the three fundamental supermodes of the three-waveguide structure was shown in Fig.3(b). The supermodes that involved in the interference within 54 °C to 55 °C were symmetric mode and decoupling mode with index contrast at $\Delta n = 0.0014149$, and simulated temperature sensitivity is 35.2263 nm/°C.The same simulation method can be introduced within temperature range from 55 °C to 58.2 °C. Simulation revealed the interference pattern generated by two higher order supermode with refractive index $\Delta n = 0.00092795$. Simulated sensitivity equaled to 19.4995nm/°C and Δn = 0.0009228. The slight difference between experimental data and the simulated results may cause by the inaccuracy when measuring the length of liquid filled TCPCF. Thus, we can conclude that the large spectrum envelop was generated by the interference between symmetric mode and decoupling mode when temperature ranges from 54 °C to 55 °C and induced by interference between higher order supermodes from 55 °C to 58.2 °C.

REFERENCES

[1] Algorri, J. F., Zografopoulos, D. C., Tapetado, A., Poudereux, D., and Sánchez-Pena, J. M. “Infiltrated Photonic Crystal Fibers for Sensing Applications,” Sensors (Basel, Switzerland), 18(12), 4263-4295 (2018).

[2] Nielsen, K., et al. "Selective filling of photonic crystal fibres," Journal of Optics A: Pure and Applied Optics 7(8), 13-20 (2005).
[3] Russell, P. “Photonic crystal fibers,” Science, 299(5605), 358-362 (2003).
[4] T. Han, Y. Liu, Z. Wang, B. Zou, B. Tai, and B. Liu, " Avoided-crossing based ultrasensitive photonic crystal fiber refractive index sensor," Opt. Lett. 35, 2061-2063 (2010).
[5] Wang, Y., et al. "Selectively Infiltrated Photonic Crystal Fiber With Ultrahigh Temperature Sensitivity," IEEE Photonics Technology Letters 23(20), 1520-1522 (2011).
[6] Yang, M. and D. N. Wang. "Photonic Crystal Fiber With Two Infiltrated Airholes for Temperature Sensing With Excellent Temporal Stability,” Journal of Lightwave Technology 30(21), 3407-3412 (2012).
[7] Jiangbing Du, Yange Liu et al. "Thermally tunable dual-core photonic bandgap fiber based on the infusion of a temperature-responsive liquid," Opt. Express 16(6), 4263-4269 (2008).
[8] Gao, R., et al. "Magnetic Fluid-Infiltrated Anti-Resonant Reflecting Optical Waveguide for Magnetic Field Sensing Based on Leaky Modes," Journal of Lightwave Technology 34(15), 3490-3495 (2016).
[9] Hu, D. J. J., et al. "Fabrication and Characterization of a Highly Temperature Sensitive Device Based on Nematic Liquid Crystal-Filled Photonic Crystal Fiber,” IEEE Photonics Journal 4(5), 1248-1255 (2012).
[10] Zhilin Xu., et al. “Hybrid photonic crystal fiber for highly sensitive temperature measurement,” J. Opt. 20(7), 075801-075807 (2018).
[11] Gao, R., et al. "Temperature-compensated fibre optic magnetic field sensor based on a self-referenced anti-resonant reflecting optical waveguide,” Appl. Phys. Lett.110(13), 131903-131908 (2017).
[12] T. Han, Y. Liu, Z. Wang, B. Zou, B. Tai, and B. Liu, "Avoided-crossing based ultrasensitive photonic crystal fiber refractive index sensor. " Opt. Lett. 35, 2061-2063 (2010).
[13] Hou, M., et al. "Multi-Components Interferometer Based on Partially Filled Dual-Core Photonic Crystal Fiber for Temperature and Strain Sensing,” IEEE Sensors Journal 16(16), 6192-6196 (2016).
[14] Yan Yan and Jean Toulouse, "Nonlinear inter-core coupling in triple-core photonic crystal fibers," Opt. Express 17(22), 20272-20281 (2009).
[15] Allan W. Snyder, "Coupled-Mode Theory for Optical Fibers," J. Opt. Soc. Am. 62(11), 1267-1277 (1972).
[16] Yan Yan, Jean Toulouse, Iavor Velchev, and Slava V. Rotkin, "Decoupling and asymmetric coupling in triple-core photonic crystal fibers," J. Opt. Soc. Am. B 25(9), 1488-1495 (2008).
[17] Liu, Q., Li, S., Chen, H., Li, J., & Fan, Z. “High-sensitivity plasmonic temperature sensor based on photonic crystal fiber coated with nanoscale gold film,” Applied Physics Express 8(4), 046701-046705 (2015).
[18] Hu, Dora Juan Juan, Rebecca Yen-Ni Wong, and Perry Ping Shum, "Photonic Crystal Fiber-Based Interferometric Sensors," Selected Topics on Optical Fiber Technologies and Applications. InTech, 21-41 (2018).
[19] Y. Wang, Y. Li, C. Liao, D. N. Wang, M. Yang and P. Lu, "High-Temperature Sensing Using Miniaturized Fiber In-Line Mach–Zehnder Interferometer," in IEEE Photonics Technology Letters 22(1), 39-41 (2010).
[20] Liang, H., et al. "Fiber in-line Mach-Zehnder interferometer based on near-elliptical core

photonic crystal fiber for temperature and strain sensing," Opt. Lett. 38(20), 4019-4022 (2013).
[21] D. K. C. Wu, B. T. Kuhlmey, and B. J. Eggleton, "Ultrasensitive photonic crystal fiber refractive index sensor," Opt. Lett. 34(3), 322-324 (2009).
[22] Hou, M., et al. "Multi-Components Interferometer Based on Partially Filled Dual-Core Photonic Crystal Fiber for Temperature and Strain Sensing," IEEE Sensors Journal 16(16), 6192-6196 (2016).
[23] Qian, W., Zhao, C. L., He, S., Dong, X., Zhang, S., Zhang., "High-sensitivity temperature sensor based on an alcohol-filled photonic crystal fiber loop mirror," Opt. Lett. 36(9), 1548-1550 (2011).
[24] Jauregui-Vazquez, D., et al. "Modified All-Fiber Fabry–Perot Interferometer and Its Refractive Index, Load, and Temperature Analyses," IEEE Photonics Journal 7(3), 1-9 (2015).
[25] Luo, H., et al. "Simultaneous measurement of refractive index and temperature using multimode microfiber-based dual Mach-Zehnder interferometer," Opt. Lett. 39(13), 4049-4052 (2014).